Journal of Applied Polymer Science

Fabrication and Modification of Acrylonitrile–Butadiene–Styrene-Based Heterogeneous Ion-Exchange Membranes by Plasma Treatment: Investigation of the Nanolayer Deposition Rate and Temperature Effects

Akbar Zendehnam,[1] Nasrin Robatmili,[1] Sayed Mohsen Hosseini,[2] Mina Arabzadegan,[1] Sayed Siavash Madaeni[3]

[1]Thin Film Laboratory, Department of Physics, Faculty of Science, Arak University, Arak 38156-8-8349, Iran

[2]Department of Chemical Engineering, Faculty of Engineering, Arak University, Arak 38156-8-8349, Iran

[3]Membrane Research Centre, Department of Chemical Engineering, Faculty of Engineering, Razi University, Kermanshah 67149, Iran

Correspondence to: S. M. Hosseini (E-mail: sayedmohsen_hosseini@yahoo.com or s-hosseini@araku.ac.ir) or A. Zendehnam (E-mail: A-zendehnam@araku.ac.ir)

ABSTRACT: Our target in this study was the preparation of electrodialysis ion-exchange membranes with appropriate properties for applications in water recovery and treatment. Composite mixed-matrix, anion-exchange membranes were prepared by a solution casting technique with acrylonitrile–butadiene–styrene as a base binder, resin powder as a functional group agent, activated carbon as an adsorptive filler, and an Ag nanolayer as a surface modifier. The Ag nanolayer was used with a magnetron sputtering method. The effect of the nanolayer deposition rate (R_q) and substrate and annealing temperatures on the physicochemical characteristics of the membranes were studied. The X-ray diffraction results show that average grain size of the nanolayer and membrane crystallinity were improved with increasing R_q. The atomic force microscopy and scanning electron microscopy results show that the membrane roughness was enhanced with increasing R_q. The height distribution results also show the best height distribution for the modified membrane at low R_q. The selectivity and flux decreased with increasing nanolayer R_q in the membranes. The selectivity was also decreased initially with increases in the substrate and annealing temperatures from 300 to 325 K in the membranes and then showed an increasing trend. An opposite trend was found for flux with variations in the temperature. The modified membrane containing a 20-nm Ag nanolayer at low R_q showed better performance compared to the other modified membranes and the pristine one.

 J. Appl. Polym. Sci. **2014**, *131*, 40025.

KEYWORDS: ion exchange membrane; plasma treatment; nanolayer deposition rate; temperature effect; synergy phenomenon

Received 21 June 2013; accepted 1 October 2013

DOI: 10.1002/app.40025

INTRODUCTION

Nowadays, membrane technology is widely used in separation processes, and so various membranes have been developed.[1,2] Among these, ion-exchange membranes (IEMs) are one of the most advanced separation membranes. A shortage of water is a serious problem all over the world because of population growth and the expansion of industrial activities. Therefore, there is a growing impetus for wastewater recycling and reuse. IEMs are efficient tools for recovery and treatment processes.[3–5]

The successful applications of IEMs include conventional electrodialysis for cleaner production and treating separation,[6–10] diffusion dialysis to acid recovery, and Donnan dialysis to remove hazardous elements.[11] Also, they can be used in acidic gas separation, protein purification, and the enrichment of elements or solid electrolytes in alkaline fuel cells.[12–16] The removal of harmful ions from groundwater has also attracted much attention as an aspect of human health.[17–20]

Membrane processes require membrane development with appropriate properties, such as a high selectivity[21,22] and flux and a suitable amount of energy consumption, which can be raised by changes in the membrane physicochemical characteristics.[23,24] Also, the use of solid polymer electrolytes represents

another method to follow for IEMs, especially those used in fuel cell research.[25–27]

The development of novel methods for membrane modification is an important issue. Various methods, such as UV irradiation, plasma treatment, γ irradiation, and chemical reactions, have been used in modification processes.[28–30] Among these techniques, plasma treatment is regarded as the most advantageous.[31] In this process, the generated active species in plasma conditions can activate the upper molecular layers on the membrane surface without affecting the bulk of the membrane.[30,32]

The preparation of heterogeneous IEMs with appropriate properties for application in electrodialysis processes related to water recovery and treatment was the primary target of this research. For this purpose, acrylonitrile–butadiene–styrene (ABS)-based IEMs were prepared by a solution casting technique with anion-exchange resin powder as a functional group agent and tetrahydrofuran as a solvent. Activated carbon (AC) and Ag nanolayers were also used as an adsorptive filler and surface modifier, respectively.

The application of copolymers and terpolymers, such as ABS, in the process of membrane fabrication can provide the necessary potential to improve the membranes properties. This is attributed to the combined rubbery and glassy characteristics in ABS.[33–35] AC was also used as an inorganic filler additive in membrane fabrication to create adsorptive active sites in the membrane matrix, which provided an attractive alternative for capitalizing on the membranes' superior separation properties.[35] The use of nanomaterials in polymeric matrices has also been examined in many applications to improve the physicochemical properties, such as the thermal and oxidative stabilities, biofouling, and antibacterial and separation characteristics on the basis of the synergism between the organic and inorganic component properties.[33–39] In recent years, silver nanomaterials have been used extensively in membrane characterization because of their interesting features and capacity, such as their superior electrical and thermal conductivity and antimicrobial effects.[33,36,37]

Ag nanolayer was also deposited on the membrane surface by an radio frequency (RF) magnetron sputtering method. The effect of the Ag nanolayer deposition rate (R_q; low: 0.65 nm/s, medium: 1.35 nm/s, and high: 2.8 nm/s) and the substrate and annealing temperatures (300–350 K) on the physicochemical characteristics of the membranes were also studied.

EXPERIMENTAL

Materials

ABS [density = 1.04 gr/cm^3, melt flow rate (MFR) (ASTMD 1238) = 1.7 g/10 min, tensile strength yield (ASTM D 638) = 440 Kgf/cm^2, flexural strength yield (ASTM D 790) = 640 Kgf/cm^2, flexural modulus (ASTM D 790) = 20,500 Kgf/cm^2, softening temperature (ASTM D 1525) = 99°C, glass-transition temperature $\approx$ 107°C, Tabriz Petrochemical Corp., Iran] was used as a binder. Tetrahydrofuran was used as a solvent. AC (powder, extrapure), as an inorganic filler additive and anion-exchange resin (Amberlite IRA-402, strongly basic anion exchanger, Cl form, Merck), was applied to prepare the membranes. Silver (Ag) with a high purity (99.9%) and argon (research grade, 99.9%) were also used as target and plasma formers, respectively, in the magnetron sputtering system. All of the other chemicals were supplied by Merck. Throughout the experiments, distilled water was used.

Fabrication of the IEMs

The anion-exchange membranes were prepared by a solution casting technique, as described earlier.[33–35] The membranes were prepared by the dissolution of ABS in tetrahydrofuran (1:16 w/w) in a glass reactor equipped with a mechanical stirrer for more than 4 h. This was followed by the dispersal of a specific quantity of ground resin particles (size = −300 to +400 mesh) as functional group agents (resin: 50 wt % ABS) and AC as an inorganic filler additive (2.0 wt %) in the polymeric solution. The mixture was mixed vigorously at room temperature to obtain a uniform particle distribution in the polymeric solution. In addition, for the better dispersion of particles, the solution was sonicated with an ultrasonic instrument (Pars Nahand Engineering Co., 150 W). The mixture was then cast onto a clean, dry glass plate. The membranes were dried at ambient temperature (relative humidity = 28%) for 1 h and then immersed in distilled water (26°C bath temperature). In the final stage, the membranes were pretreated by immersion in a 1*M* NaCl solution. The membrane thickness was measured with a digital caliper device. The membrane thickness was around 100–120 μm.

The Ag-coated membranes were prepared by plasma treatment. After the impurities were removed, the prepared membrane were coated with silver nanoparticles in a vacuum reactor (with 10^{-6} mbar of base pressure) by argon plasma treatment with a magnetron sputtering method (planar magnetron sputtering, Model: 12″ MSPT; Make: Hind High Vaccum Co.Pvt.Ltd, Bangalore, India) at 90 W of power (direct-current magnetron power supply, model PS-2000). Suitable adhesions of the film to the substrate, uniformity, good and controllable R_q, and high purity are some of advantages of this method. Silver with a high purity (99.9%) and argon (research grade, 99.9%) were used as target and plasma formers, respective, in the magnetron sputtering system. The distance between the membrane (substrate) and silver target (cathode, 12.5 cm in diameter and 3 mm in thickness) was kept at 12 cm (optimal distance) in the plasma reactor during the process to obtain a uniform film with a good packing density. R_q of the silver layer was expressed as follows:[40]

$$R_q = K\frac{P_E}{Pd}, P_E = VI \quad (1)$$

where P is the gas pressure, d is the distance between the target (Ag cathode) and anode (substrate holder), P_E is the electrical power, K is a constant that depends on the type of gas and target material, V is the voltage, and I is the electrical flow.

The variation of R_q against P_E is shown Figure 1. A linear plot was obtained, as we expected. We adjusted the thickness of the coating nanolayer by changing the deposition time (with a ±2 nm instrument error). Before starting the actual experiment, we

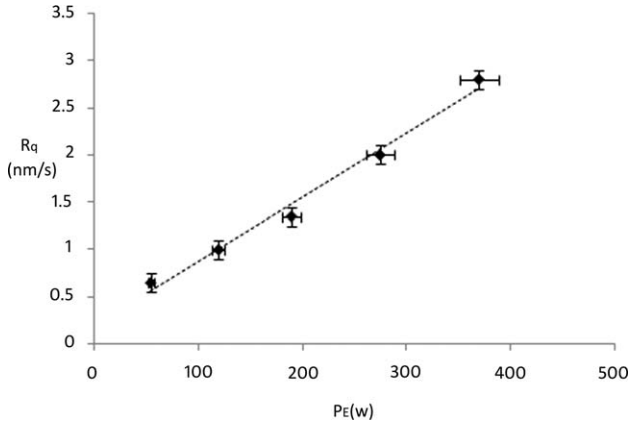

Figure 1. R_q versus P_E.

presputtered the target for 10 min with a moveable shutter located between the target and the substrate. This shutter was also used to control the period of the deposition exactly. In fact, after the expiration of a specific deposition time, the moveable shutter was placed between the target and the substrate, and this prevented more deposition.

Test Cell

The electrochemical property measurements were carried out with a test cell, as reported earlier (Figure 2).[33–35] The cell consisted of two cylindrical compartments made of Pyrex glass separated by the membrane. One side of each vessel was closed by a Pt electrode supported with a piece of Teflon, and the other side was equipped with a piece of porous medium to support the membrane. To minimize the effect of the boundary layer during the experiments, both sections were stirred vigorously by magnetic stirrers.

Membrane Characterization

Atomic Force Microscopy (AFM). AFM was used to analyze the surface morphology and the roughness of the prepared membranes under contact mode. The AFM device was a dual-scope scanning probe-optical microscope (DME 95–200e). Small pieces of the prepared membranes (~1 cm^2) were used.

Scanning Electron Microscopy (SEM). The morphology of the prepared membranes was observed by SEM (S360 Cambridge

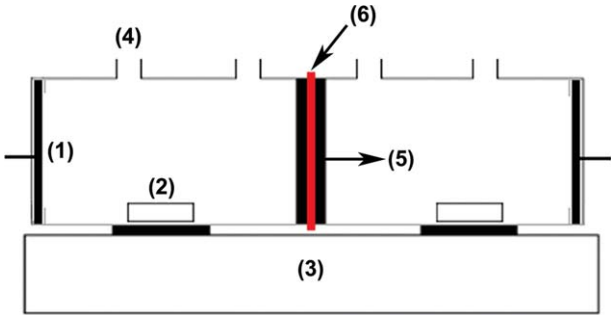

Figure 2. Schematic diagram of the membrane test cell: (1) Pt electrode, (2) magnetic bar, (3) stirrer, (4) orifice, (5) rubber ring, and (6) membrane. [Color figure can be viewed in the online issue, which is available at wileyonlinelibrary.com.]

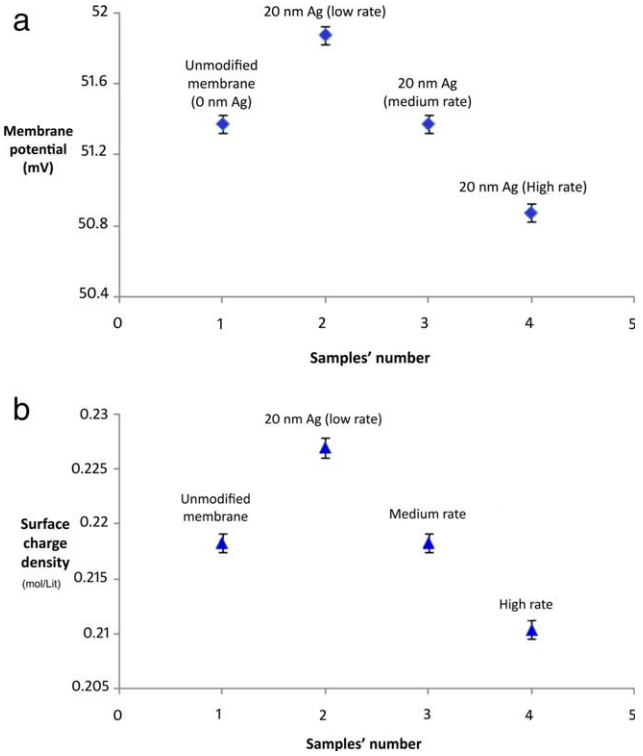

Figure 3. (a) $E_{measure}$ and (b) surface charge density of the membranes (the unmodified membrane and modified membranes with 20-nm Ag nanolayers) at various R_q's (low: 0.65 nm/s, medium: 1.35 nm/s, and high: 2.8 nm/s). [Color figure can be viewed in the online issue, which is available at wileyonlinelibrary.com.]

1990). The membranes were broken into small pieces and were then sputtered with gold.

X-ray Diffraction (XRD) Analysis. For microstructural studies of the deposited Ag nanolayer, XRD patterns were obtained with an X-ray diffractometer (model X'Pert Pw 3373, wavelength radiation (K_α) = 1.54 Å, Philips, Holland).

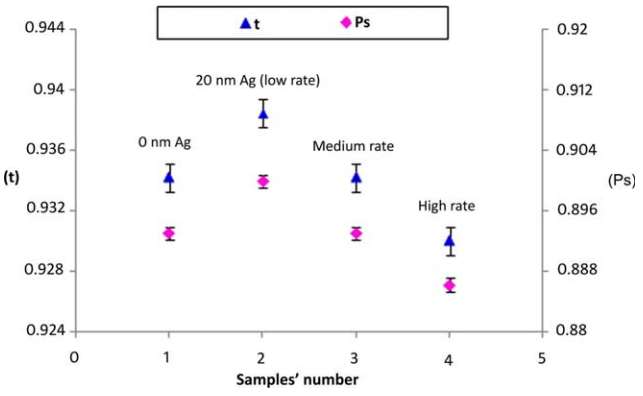

Figure 4. Permselectivity and transport number values of the membranes (unmodified membrane and modified membranes with 20-nm Ag nanolayers) at various R_q's (low: 0.65 nm/s, medium: 1.35 nm/s, and high: 2.8 nm/s). [Color figure can be viewed in the online issue, which is available at wileyonlinelibrary.com.]

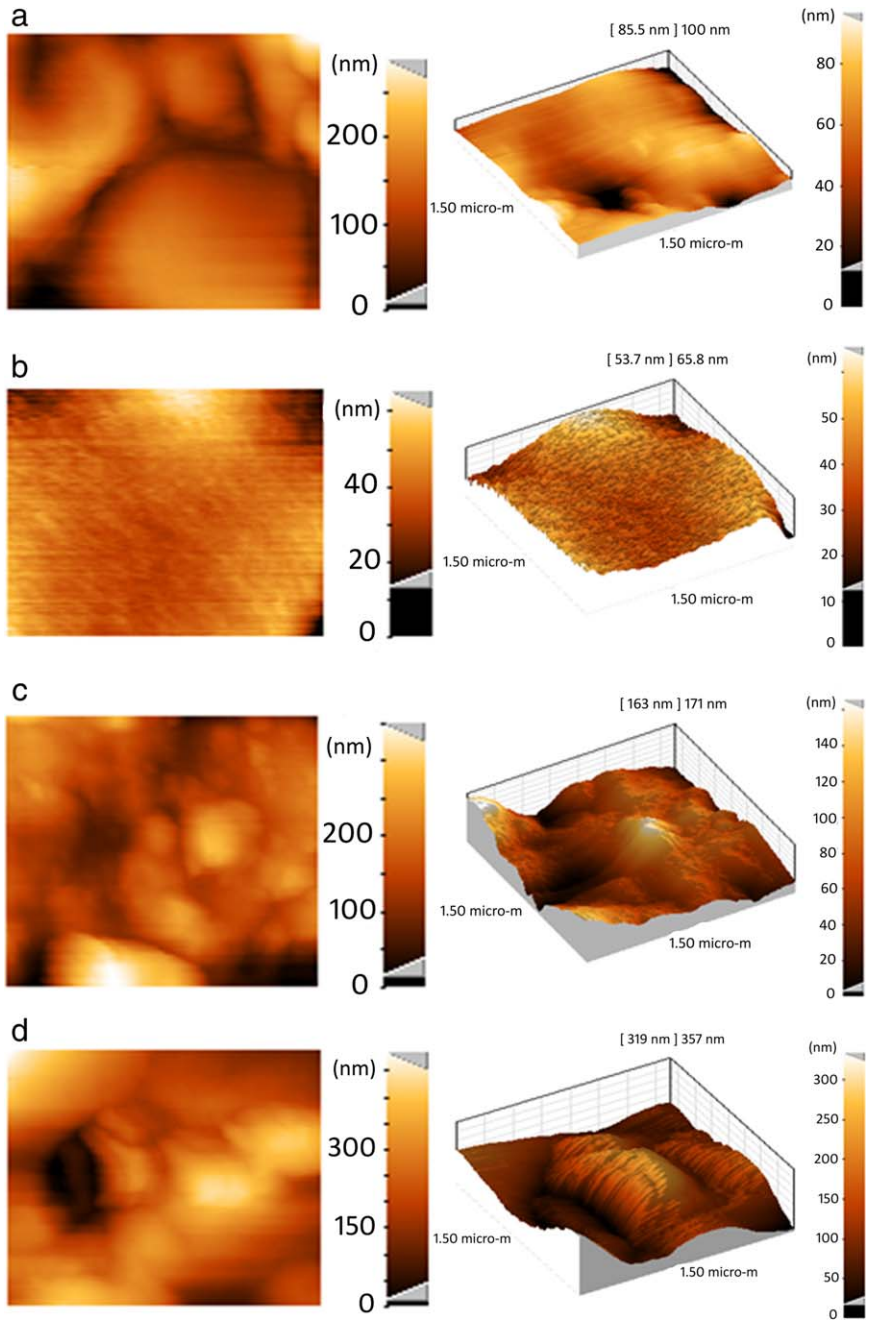

Figure 5. AFM analysis images of the IEMs: (a) pristine membrane without coating and (b–d) modified membranes with Ag nanolayer coatings: (b) low rate: 0.65 nm/s, (c) medium rate: 1.35 nm/s, and (d) high rate: 2.8 nm/s. [Color figure can be viewed in the online issue, which is available at wileyonlinelibrary.com.]

Membrane Potential ($E_{measure}$), Transport Number, and Permselectivity. The magnitude of $E_{measure}$ depends on the electrical characteristic of a membrane and the nature and concentration of the electrolyte solution.[35,41–43] This parameter was evaluated for the equilibrated membrane with unequal concentrations of sodium chloride ($C_1 = 0.1M$ and $C_2 = 0.01M$ at ambient temperature) on either side of membrane with the two-cell glassy apparatus shown in Figure 2. We measured the developed potential difference across the membrane by connecting both compartments and using a saturated calomel electrode and digital auto multimeter. The $E_{measure}$ generated is expressed with the Nernst equation[33–35,41–43] as follows:

$$E_{measure} = \left(2t_i^m - 1\right)\left(\frac{RT}{nF}\right)\ln\left(\frac{a_1}{a_2}\right) \quad (2)$$

where t^m is the transport number of counter ions in the membrane phase, R is the gas constant, T is the temperature, F is the Faraday constant, n is the electrovalence of counter ion, and a_1 and a_2 are the activities of the solution electrolyte

Table I. Membrane AFM Analysis Results and Surface Roughness and Height Values as Calculated by Danish Micro Engineering (DME) Scanning Probe Microscope (SPM) Software

Membrane	Average surface roughness (nm)	Maximum height (nm)	Average height (nm)
ABS (0.65 nm/s) + 0-nm Ag	12.6	100	80.73
ABS (0.65 nm/s) + 20-nm Ag	5.62	65.8	48.31
ABS (1.35 nm/s) + 20-nm Ag	22.6	171	54
ABS (2.8 nm/s) + 20-nm Ag	42.2	357	230

in contact with both surfaces, which are determined with the Debye–Hackle limiting law. The membrane ionic permselectivity is also expressed on the basis of the migration of the counter ion through the IEM:[33–35,41–43]

$$P_s = \frac{t_i^m - t_0}{1 - t_0} \tag{3}$$

where t_0 is the transport number of counter ions in solution[44] and P_s is the membrane permselectivity.

The concentration of fixed charge on the membrane surface (Y) is also expressed in terms of the permselectivity, as follows:[34,35,41–43]

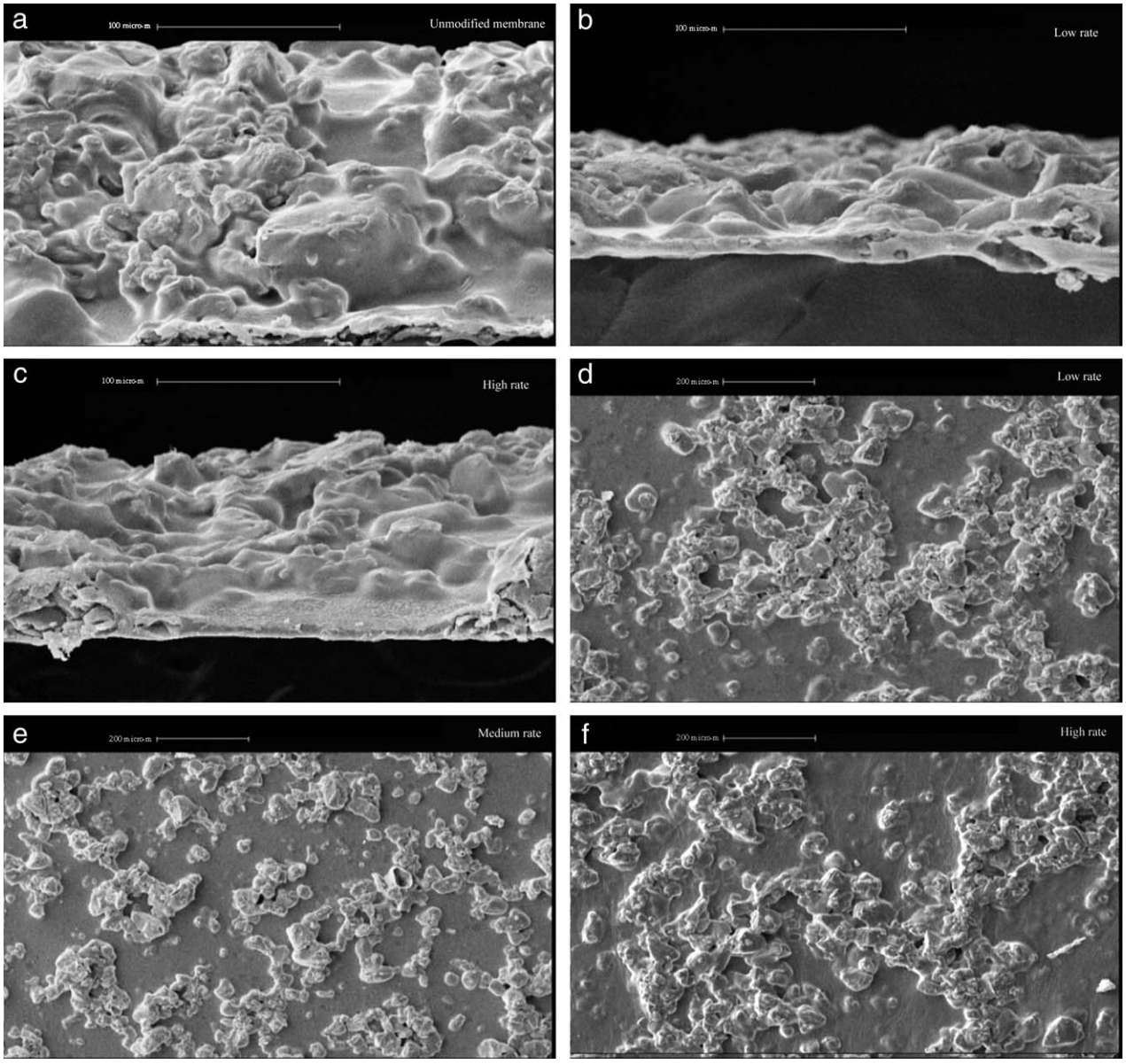

Figure 6. SEM images of the unmodified and modified membranes with nanolayer coatings at different R_q's: (a–c) cross-sectional images and (d–f) surface images.

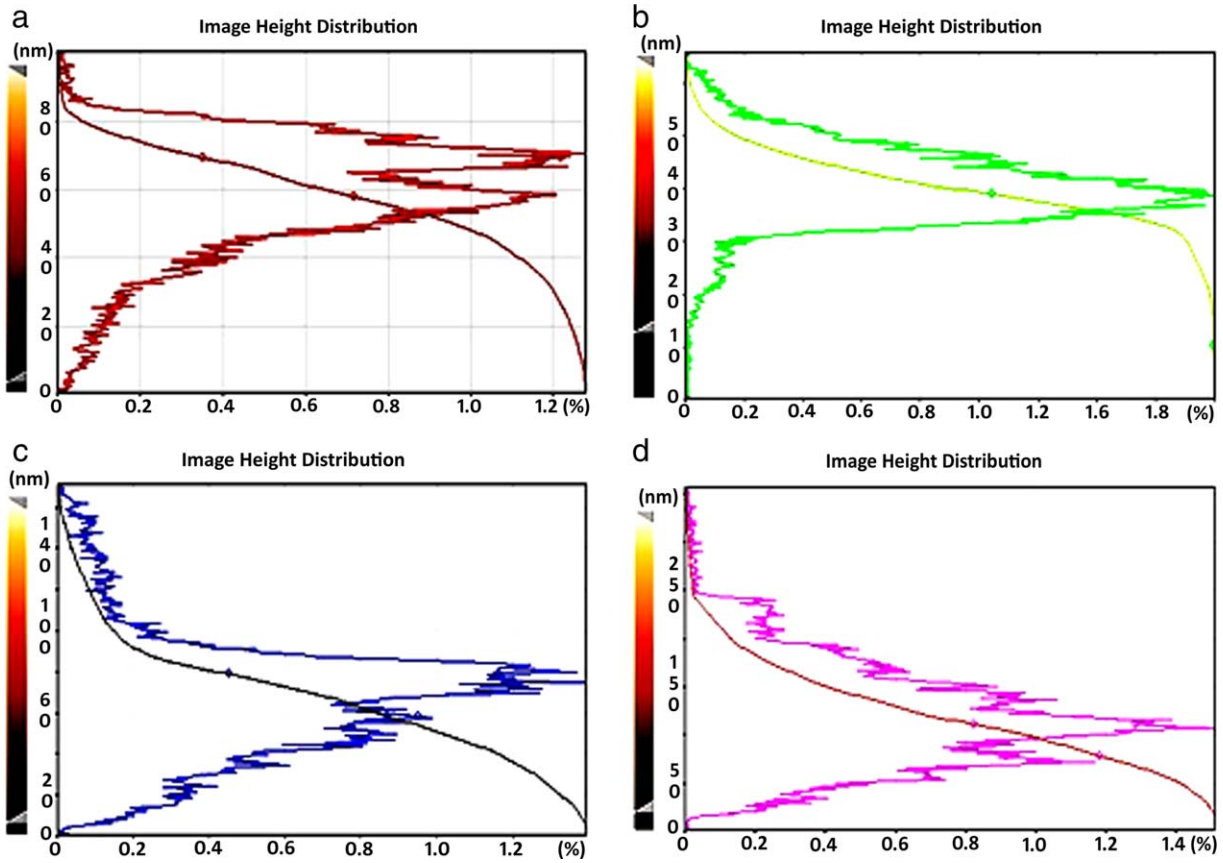

Figure 7. Height distribution analysis of the prepared membranes: (a) pristine membrane without coating and (b–d) modified membranes with 20-nm Ag nanolayers: (a) low rate: 0.65 nm/s, (b) medium rate: 1.35 nm/s, and (c) high rate: 2.8 nm/s. [Color figure can be viewed in the online issue, which is available at wileyonlinelibrary.com.]

$$Y = \frac{2C_{\text{Mean}}P_s}{\sqrt{1-P_s^2}} \tag{4}$$

where C_{mean} is the mean concentration of electrolytes (0.055M). The existence of greater conducting regions on the membrane surface can strengthen the intensity of the uniform electrical field around the membrane and decrease the polarization concentration phenomenon.[45]

Ionic Permeability and Flux. The ionic flux (N) measurement was carried out with the test cell (Figure 2). A 0.1M NaCl solution was placed on an anodic section of the cell, and a 0.01M solution was placed on its cathodic side. A direct-current electrical potential with an optimal constant voltage (10 V) was applied across the cell with stable platinum electrodes. During the experiment, both sections were recirculated and stirred vigorously to minimize the effect of the boundary layers. The cations passed through the membrane to the cathodic section. Also, according to the anodic and cathodic reactions, the produced hydroxide ions remained in the cathodic section and increased the pH of this region as follows:

$$2Cl^- \Rightarrow Cl_2 \uparrow + 2e^- \text{ (anodic reaction)}$$

$$2H_2O + 2e^- \Rightarrow H_2 \uparrow + 2OH^- \text{ (cathodic reaction)}$$

The amount of produced hydroxide ions in the cathodic section was equal to the chloride ions transported through the membrane (N). The pH changes were measured with a digital pH meter. Also according to Fick's first law, the flux of ions through the membrane can be expressed as follows:[46,47]

$$N = -P\frac{dC}{dx} = P\frac{C_1 - C_2}{d} \tag{5}$$

where P is the ionic permeability coefficient, d is the membrane thickness, and C is the ion concentration in the compartments:

$$N = -\frac{v}{A} \times \frac{dC_1}{dt} = P\frac{C_1 - C_2}{d},\ C_2 = C_2{}^0 \tag{6}$$

where A is the membrane surface area, t is the time, and v is the volume.

$$\int_{C_1{}^0}^{C_1} -\frac{dC_1}{(C_1 - C_2{}^0)} = \int_0^t P\frac{A}{vd}dt \tag{7}$$

$$\ln\frac{(C_1 - C_2{}^0)}{(C_1{}^0 - C_2{}^0)} = -\frac{PAt}{vd} \tag{8}$$

The ionic permeability coefficient (P) in the membrane phase was calculated with eq. (8). The flux was also measured with the consideration of the pH variation in the cathodic section.

It is worth mentioning that the measurements were carried out three times for each sample, and their average values were reported to minimize experimental errors.

RESULTS AND DISCUSSION

Effect of the Ag Nanolayer R_q

The effect of the Ag nanolayer R_q on the membrane physicochemical properties was studied. The obtained results reveal that $E_{measure}$, the membrane selectivity, and the transport number (Figures 3 and 4) all decreased with an increase in the nanolayer R_q in the prepared membranes. This was due to the decrease in the membrane charge density (Figure 3), which reduced the interactions between the counter ions and the membrane surface. Moreover, the AFM results (Figure 5 and Table I) show that the membrane roughness increased with increasing nanolayer R_q. This was attributed to an increase in the average grain size of the deposited nanolayer (X-ray results) and also the irregular nanoparticle position at high R_q. The increase in the membrane roughness strengthened the concentration polarization effect caused by the formation of stagnant electrolyte layers on the membrane surface and so increased the possibility of co-ion percolation. This led to lower co-ion rejection for the rough membrane compared to smooth ones and so decreased the $E_{measure}$, selectivity, and transport number. The membrane roughness parameters are shown in Table I (sample size = 1.5 × 1.5 μm^2). The SEM images (Figure 6) also confirmed the increase in roughness with increasing nanolayer R_q. The height distribution results (Figure 7) showed the best height distribution for the Ag nanolayer-coated membrane at low R_q compared to others. In Figure 7, the x axis represents the percentage of points with same height distribution, and the y axis represents the height distribution. The results were nearly Gaussian.

Furthermore, the modified membrane containing 20-nm Ag nanolayers (at low R_q) showed better $E_{measure}$, selectivity, and transport number (Figures 3 and 4) compared to pristine ones without a nanolayer coating. This was due to the electrical properties and adsorption characteristic of the silver nanoparticles, which made powerful conducting regions for the membrane and so enhanced the surface charge density [Figure 3(b)]. This provided superior electrostatic interactions of ions with the membrane surface and so facilitated the counter-ion transportation; this, in turn, led to enhanced Donnan exclusion. Moreover, the ionic pathways, cracks, and fissures on the membrane surface were occupied by the silver particles, and they were narrowed by them as space-limiting factors. This strengthened the ionic site domination on ion traffic and improved the permselectivity. The AFM and height distribution results also show a smoother surface and better height distribution for the modified membrane at low R_q compared to the pristine one.

The membrane ionic permeability coefficient and flux are shown in Figure 8(a,b). The obtained results revealed that N and the permeability coefficient decreased with increasing in nanolayer R_q. This was attributed to the increase in the membrane crystallinity (see the XRD results in Figure 9); this hindered the moieties and segments moving in the membrane matrix and compressed them more together. As a result, the ion traffic decreased.[48,49] As shown in Figure 9 (XRD spectra results), the

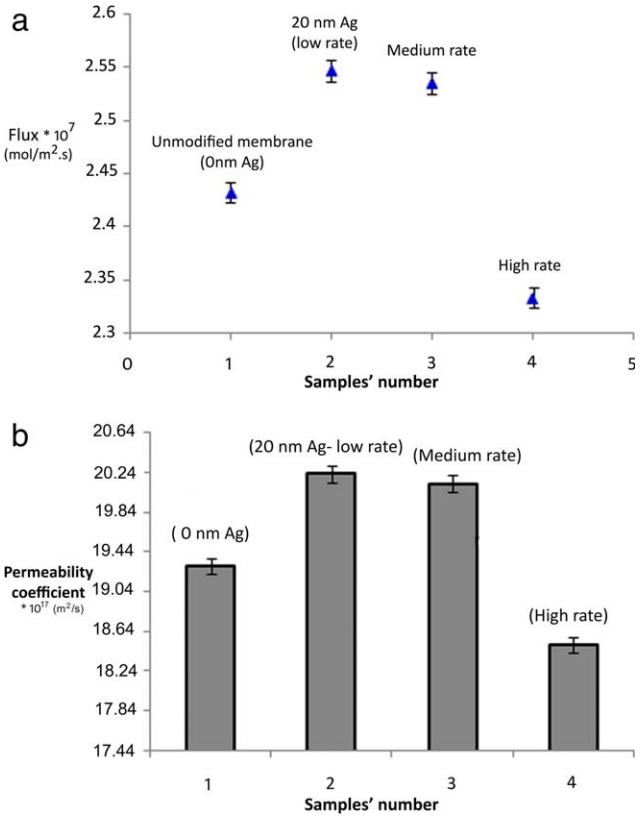

Figure 8. (a) Ionic coefficient permeability and flux: unmodified membrane and modified membranes with Ag nanolayer coatings. [Color figure can be viewed in the online issue, which is available at wileyonlinelibrary.com.]

(111) and (200) diffraction peaks appeared with increasing nanolayer R_q. The grain sizes of the deposited nanolayers (crystallite sizes) were estimated with the Scherrer formula:[40]

$$D = \frac{K\lambda}{\beta \cos\theta} \tag{9}$$

where D is the average grain size of the formed crystallite, λ is the wavelength of the X-ray used (1.54Å), β denotes the full width at half maximum for the corresponding

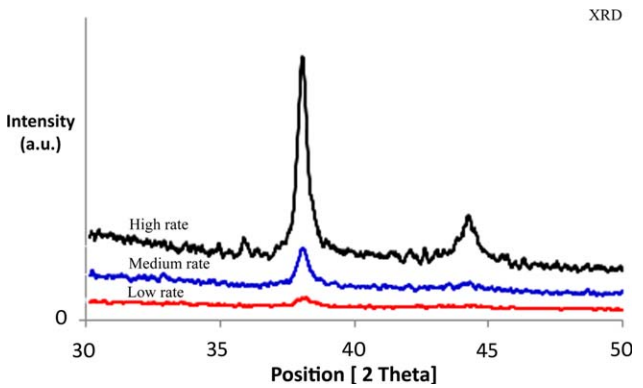

Figure 9. XRD patterns of the modified membrane and investigation of the Ag nanolayer R_q effect (low, medium and high). [Color figure can be viewed in the online issue, which is available at wileyonlinelibrary.com.]

diffraction peak, θ is the diffraction angle, and K is a constant (0.9–1).

The deposited nanolayer films exhibited a (111) orientation. We found that the average grain size of the nanolayer (crystallite size) was improved from 17.25 to 30 nm with increasing nanolayer R_q from 0.65 to 2.8 (nm/s).

The modified membrane with a 20-nm Ag nanolayer at low R_q showed a higher N and permeability coefficient [Figure 8(a,b)] compared to the pristine membranes without coating. The Ag nanolayer resulted in superior electrostatic interactions for the ions with the membrane surface and improved the permeability coefficient and the flux.

Among the prepared membranes, the modified membrane containing a 20-nm Ag nanolayer at low R_q (0.65 nm/s) showed a higher N and selectivity compared to the other modified membranes and also the unmodified ones.

A comparison between the prepared membrane in this research and some commercial membranes is given in Table II. The results show that modified membranes in this study were comparable with other commercial ones.

Effects of the Substrate and Annealing Temperatures on Membrane Performance

The results show that P_s (Figure 10) decreased initially with increasing substrate (IEM) temperature and annealing temperature form 300 to 325 K in the modified membrane. This may have been due to the Ag nanoparticles permeating the membrane matrix; this interrupted the polymer chains and, thus, decreased the membrane selectivity. The selectivity was enhanced in the modified membranes with another increase in the temperature form 325 to 350 K. This may have been due to a membrane structure shrinkage phenomenon, which reduced the pore and fissure sizes in the membrane matrix[50] and, thus, strengthened the ionic site domination on ion traffic. This enhanced the membrane selectivity. The pristine membranes similarly showed an increasing selectivity with increasing treatment temperature because of the membrane structure shrinkage phenomenon.

The obtained results reveal that N [Figure10(b)] was also initially enhanced with the increase in the temperature up to 325 K in the modified membrane and then showed a decreasing trend with a greater increase in the temperature to 350 K. These phenomena could be explained with respect to the interruption of the polymer chains and the membrane structure shrinkage, respectively, as mentioned previously. The structure shrinkage reduced the pores and fissures sizes and so declined the ions transportation.

Table II. Comparison between the Permselectivity of the Prepared Membranes in This Study and Some Commercial Membranes [51]

Membrane	Permselectivity
Superior homemade membrane (20-nm Ag nanolayer and low R_q) [a]	90
Ralex (heterogeneous) AM or AMH - PES (Anion exchange membrane- Polyester)	>90
Fumasep FAD (Fumaseb Acid Dialysis)	>91

[a] The modified membrane with the Ag nanolayer coating exhibited antibacterial characteristics.

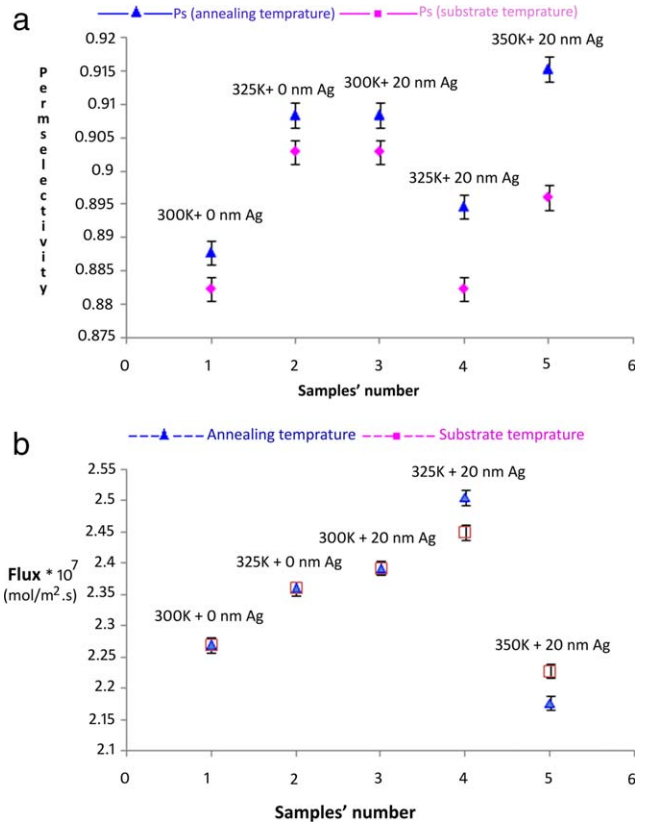

Figure 10. Effect of the substrate (IEMs) and annealing temperatures on the (a) P_s and (b) flux values of membranes: pristine membrane without a nanolayer and modified ones with 20-nm Ag nanolayer coatings. [Color figure can be viewed in the online issue, which is available at wileyonlinelibrary.com.]

CONCLUSIONS

The XRD results reveal that the average grain size of the Ag nanolayer was enhanced by an increase in the nanolayer R_q. The AFM and SEM results also show that the membrane roughness was enhanced with increasing nanolayer R_q. The height distribution results show the best height distribution for the Ag-nanolayer-coated membrane at low R_q compared to the others. The $E_{measure}$, selectivity, and flux all decreased with increasing nanolayer R_q in the modified membranes. We found that the membrane selectivity decreased initially with increasing substrate and annealing temperature form 300 to 325 K in the modified membranes and then showed an increasing trend with more increases in the temperature up to 350 K. The opposite trend was found for flux with variations in the temperature. The modified membrane containing a 20-nm Ag nanolayer (low R_q) showed better performance compared to the other modified membranes and the pristine one without a nanolayer coating.

ACKNOWLEDGMENTS

The authors gratefully acknowledge Arak University and also Iran Nanotechnology Initiative Council for financial support during this research.

REFERENCES

1. Handbook of Separation Science; Seno, M., Takagi, M., Takeda, K., Teramoto, M., Hashimoto, T., Eds.; Kyoritsu Shuppan: Tokyo, **1993**.
2. Sata, T. *J. Membr. Sci.* **2000**, *167*, 1.
3. Fuchs, W.; Binder, H.; Mavrias, G.; Braun, R. *Water Res.* **2003**, *37*, 902.
4. Kang, I. J.; Yoon, S. H.; Lee, C. H. *Water Res.* **2002**, *36*, 1803.
5. Stefan, H.; Walter, T. *J. Biotechnol.* **2001**, *92*, 95.
6. Gander, M.; Jefferson, B.; Judd, S. *Sep. Purif. Technol.* **2000**, *18*, 119.
7. Huang, C. H.; Xu, T. W.; Zhang, Y. P.; Xue, Y. H.; Chen, G. W. *J. Member. Sci.* **2007**, *288*, 1.
8. Bazinet, L. *Crit. Rev. Food Sci. Nutr.* **2005**, *45*, 307.
9. Huang, C. H.; Xu, T. W. *Environ. Sci. Technol.* **2006**, *40*, 5233.
10. Saracco, G. *Ann. Chim. Rome* **2003**, *93*, 817.
11. Xu, T.; Liu, Z.; Li, Y.; Yang, W. *J. Membr. Sci.* **2008**, *320*, 232.
12. Kalbfuss, B.; Wolff, M.; Geisler, L.; Tappe, A.; Wickramasinghe, R.; Thom, V.; Reichl, U. *J. Membr. Sci.* **2007**, *299*, 251.
13. Syrén, P. O.; Rozkov, A.; Schmidt, S. R.; Stromberg, P. *J. Chromatogr. B* **2007**, *856*, 68.
14. Karppi, J.; Akerman, S.; Akerman, K.; Sundell, A.; Nyyssonen, K.; Penttila, I. *Int. J. Pharm.* **2007**, *338*, 7.
15. Qian, P.; Schoenau, J. *J. Pedosphere* **2007**, *17*, 77.
16. Linker, R.; Shaviv, A. *Appl. Spectrosc.* **2006**, *60*, 1008.
17. Tor, A. *J. Hazard. Mater.* **2007**, *141*, 814.
18. Rautenbach, R.; Kopp, W. *Desalination* **1987**, *65*, 241.
19. Indusekhar, V. K.; Trivedi, G. S.; Shah, B. *Desalination* **1991**, *84*, 213.
20. Meller, R. B.; Ronnenberg, J.; Campbell, W. H.; Diekmann, S. *Nature* **1992**, *355*, 717.
21. Sata, T.; Mine, K.; Higa, M. *J. Membr. Sci.* **1998**, *141*, 137.
22. Eyal, A.; Kedem, O. *J. Membr. Sci.* **1998**, *38*, 101.
23. Sata, T. Ion Exchange Membranes: Preparation, Characterization, Modification and Application; The Royal Society of Chemistry: Cambridge, United Kingdom, 2004.
24. Sata, T.; Yamaguchi, T.; Matsusaki, K. *J. Phys. Chem. B* **1995**, *99*, 875.
25. Varcoe, J. R.; Slade, R. C. T.; Yee, E. L. H.; Poynton, S. D.; Driscoll, D. J.; Apperley, D. C. *Chem. Mater.* **2007**, *19*, 2686.
26. Huang, A. B.; Xia, C. Y.; Xiao, C. B.; Zhuang, L. *J. Appl. Polym. Sci.* **2006**, *100*, 2248.
27. Varcoe, J. R.; Slade, R. C. T. *Fuel Cells* **2005**, *5*, 187.
28. Rajam, S.; Ho, C. C. *J. Membr. Sci.* **2006**, *281*, 211.
29. Kim, H. I.; Kim, S. S. *J. Membr. Sci.* **2006**, *286*, 193.
30. Yu, H.-Y.; Liu, L.-Q.; Tang, Z.-Q.; Yan, M.-G.; Gu, J.-S.; Wei, X.-W. *J. Membr. Sci.* **2008**, *311*, 216.
31. Yan, M.-G.; Liu, L.-Q.; Tang, Z.-Q.; Huang, L.; Li, W.; Zhoub, J.; Gu, J.-S.; Wei, X.-W.; Yu, H.-Y. *Chem. Eng. J.* **2008**, *145*, 218.
32. Kang, M. S.; Chun, B.; Kim, S. S. *J. Appl. Polym. Sci.* **2001**, *81*, 1555.
33. Hosseini, S. M.; Madaeni, S. S.; Khodabakhshi, A. R.; Zendehnam, A. *J. Membr. Sci.* **2010**, *365*, 438.
34. Hosseini, S. M.; Madaeni, S. S.; Khodabakhshi, A. R. *J. Membr. Sci.* **2010**, *351*, 178.
35. Hosseini, S. M.; Madaeni, S. S.; Khodabakhshi, A. R. *J. Appl. Polym. Sci.* **2010**, *118*, 3371.
36. Ma, N.; Fan, X.; Quan, X.; Zhang, Y. *J. Membr. Sci.* **2009**, *336*, 109.
37. Duran, N.; Marcato, P. D.; De Souza, G. I. H.; Alves, O. L.; Esposito, E. *J. Biomed. Nanotechnol.* **2007**, *3*, 203.
38. Xu, T. *J. Membr. Sci.* **2005**, *263*, 1.
39. Thomassin, J. M.; Kollar J.; Caldarella, G.; Germain, A.; Jerome, R.; Detrembleur, C. *J. Membr. Sci.* **2007**, *303*, 252.
40. Erertovr, L. Physics of Thin Films, 2nd ed.; Plenum: New York, **1986**.
41. Nagarale, R. K.; Shahi, V. K.; Thampy, S. K.; Rangarajan, R. *React. Funct. Polym.* **2004**, *61*, 131.
42. Shahi, V. K.; Thampy, S. K.; Rangarajan, R. *J. Membr. Sci.* **1999**, *158*, 77.
43. Nagarale, R. K.; Gohil, G. S.; Shahi, V. K.; Rangarajan, R. *Colloid Surf. A* **2004**, *251*, 133.
44. Lide, D. R. CRC Handbook of Chemistry and Physics, 87th ed.; CRC: Boca Raton, FL, **2006**.
45. Kang, M. S.; Choi, Y. J.; Choi, I. J.; Yoon, T. H.; Moon, S. H. *J. Membr. Sci.* **2003**, *216*, 39.
46. Li, X.; Wang, Z.; Lu, H.; Zhao, C.; Na, H.; Zhao, C. *J. Membr. Sci.* **2005**, *254*, 147.
47. Kerres, J.; Cui, W.; Disson, R.; Neubrand, W. *J. Membr. Sci.* **1998**, *139*, 211.
48. Lin, H.; Freeman, B. D. *J. Mol. Struct.* **2005**, *739*, 74.
49. Ebadi Amooghin, A.; Sanaeepur, H. R.; Moghadassi, A. R.; Kargari, A.; Ghanbari, D.; Sheikhi Mehrabadi, Z. *Sep. Sci. Technol.* **2010**, *45*, 1385.
50. Kiyono, R.; Koops, G. H.; Wessling, M.; Strathmann, H. *J. Membr. Sci.* **2004**, *231*, 109.
51. Dlugolecki, P.; Nymeijer, K.; Metz, S.; Wessling, M. *J. Membr. Sci.* **2008**, *319*, 214.